CRATER PROJECTION IN LINEAR PUSHBROOM CAMERA IMAGES

Michela Mancini[1,*] and Carl De Vries[1] and Ava Thrasher[1] and John Christian[1,†]; [1]Guggenheim School of Aerospace Engineering, Georgia Institute of Technology, Atlanta, GA 30364., *[mmancini32@gatech.edu], †[john.a.christian@gatech.edu]

Abstract. *Science images of the Moon and Mars are often captured with pushbroom cameras. Craters with elliptical rims are common objects of interest within the the images produced by such sensors. This work provides a framework to analyze the appearance of crater rims in pushbroom images. With knowledge of only common ellipse parameters describing the crater rim, explicit formulations are developed and shown to be convenient for drawing the apparent crater in pushbroom images. Implicit forms are also developed and indicate the orbital conditions under which craters form conics in images. Several numerical examples are provided which demonstrate how different ellipse formulations can be interpreted and used in practice.*

Introduction. Pushbroom cameras are common science instruments. These sensors have a long history of imaging the surfaces of many planetary bodies, such as the Moon and Mars. Contemporary examples of pushbroom cameras within the context of planetary exploration include the Mars Express High Resolution Stereo camera,[1] the Mars Reconnaissance Orbiter (MRO) High Resolution Imaging Science Experiment (HiRISE),[2] and the Lunar Reconnaissance Orbiter Camera's (LROC) Narrow Angle Camera (NAC).[3] Pushbroom images are formed as a sequence of projective one-dimensional (1-D) images captured by a linear array of detectors. The two-dimensional (2-D) image is formed as the camera passes over the terrain. The pushbroom camera is aptly named for the sensor's motion as it sweeps out the area it images.

Pushbroom cameras are not commonly used for real-time applications (e.g., optical navigation) because of the procedure required to assemble a sequence of 1-D scans into a full 2-D image. They do, however, provide several benefits for capturing scientific images for post-flight analysis. Historically, pushbroom cameras had an advantage of not containing moving mechanical parts which may fail during the mission lifetime. However, this oft-cited advantage is less important today with the widespread incorporation of digital shutter technologies in conventional cameras. Instead, the most important modern advantage is that pushbroom cameras tend to collect more radiometrically accurate images. Each detector in the linear array is constantly exposed to the scene (compared to digital cameras or whiskbroom cameras which have finite exposure times). These longer exposure times (or "dwell times") can result in a larger scene radiance captured on individual detectors—which is particularly important under poor or variable illumination conditions.[4] In practice, the raw pushbroom images are downlinked to Earth and refined offline (e.g. radiometric correction and applying standard map projections). The construction of world maps or digital elevation maps (DEMs) are two common applications of pushbroom images.

Nearly all pushbroom imagery is captured from a low emission angle. One example is shown in Fig. 1, where we see the raw pushbroom image of a terrain patch in Mare Crisium across the top with a magnified view of Curtis crater below. This is one example of the Moon's large population of craters. Many of these craters (as well as those on Mars) have been cataloged.[6,7] While no crater is perfectly elliptical, analysis has shown that the assumption fits well with current observations.[8,9]

Now, the appearance of a planar conic (e.g. an ellipse) in an image taken by a central perspective camera (modeled as a pinhole camera) is known to be another conic. The conic to conic mapping is governed by a homography which is well understood from projective geometry.[10] In fact, this result has been utilized for several types of spacecraft optical navigation, such as crater-based[8] and horizon-based[11] methods. Unfortunately, the analytical frameworks available for pushbroom cameras are not as mature as those for central projection cameras. Full pushbroom camera models are intractable for analytical analysis due to the complexities introduced by the spacecraft's orbital motion.[12] The linear pushbroom model was developed to address some of these complexities,[13] and it
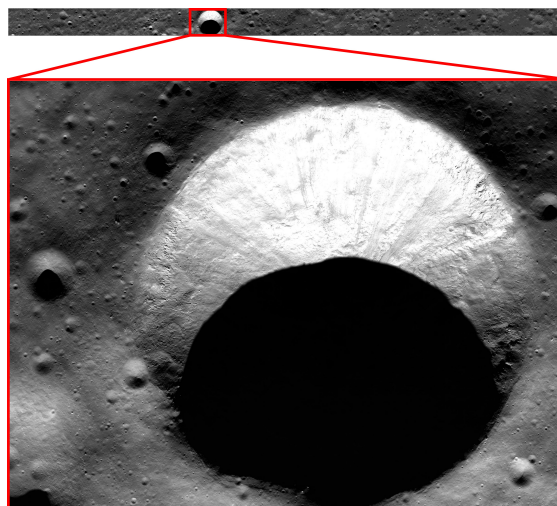
Figure 1. Pushbroom cameras tend to produce slender images with the along-track dimension much larger than the cross-track dimension due to the orbital motion. For scale, Curtis crater is approximately 2.9 km in diameter. (NASA PDS product M1323712937RE).[5]

led to insights into the formation of pushbroom images including the mapping of lines on a plane to hyperbolas in an image.

In this work we describe an analytical framework to interpret the appearance of ellipses (e.g. craters) in pushbroom cameras. We approach this work by first reviewing several mathematical formulations of ellipses. Specifically, explicit forms are developed for their convenient mapping from world coordinates to the pushbroom image plane as well as their practical use drawing ellipses using only common ellipse parameters (semi-major axis and semi-minor axis). In addition, we utilize implicit forms to 1) show that in general ellipses map to 4th order polynomials in pushbroom pixel coordinates $u-v$ and 2) provide a comprehensive treatment of the conditions under which an ellipse maps to another conic in the image plane.
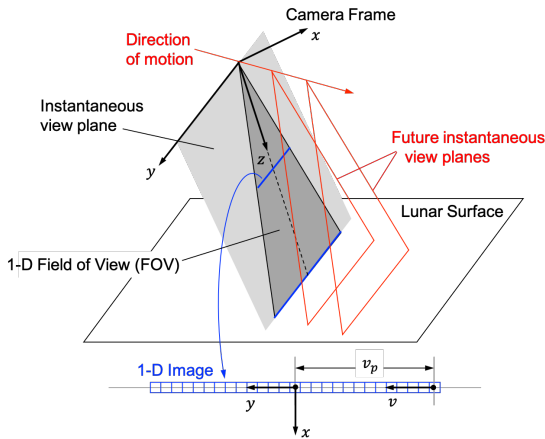
Linear Pushbroom Cameras. A pushbroom camera is an optical sensor with a 1-D detector array following perspective projection. Thus, at any instant in time, a 1-D image is formed by the perspective projection of objects residing within the instantaneous view plane (see Fig. 2). The instantaneous view plane is formed by the union of the camera location (a point) and the 1-D sensor strip (a line). As the sensor moves, the instantaneous view plane also moves and sweeps out a region of space. Stacking a sequence of 1-D images one after another creates a 2-D image.

Following the conventions of Hartley and Gupta,[13] we define a *linear* pushbroom camera to describe the scenario when the camera moves at a constant velocity and maintains a constant attitude. We will now develop the linear pushbroom model.

Begin by defining the vector $\boldsymbol{\ell}$ as the location of a world point $\boldsymbol{p}$ relative to the camera at $\boldsymbol{r}$,

$$\boldsymbol{\ell} = \boldsymbol{p} - \boldsymbol{r} \tag{1}$$

We choose to express everything in the known (and con-

Figure 2. The pushbroom camera's instantaneous view plane is the camera frame's y-z plane and contains the 1-D image formed at any instant in time.

stant) basis vectors of the camera frame. This frame has the z-direction along the boresight direction and the y-direction along the 1-D sensor strip. Thus, the instantaneous view plane is the same as the camera frame y-z plane (see Fig. 2).

Now, continue by considering the 1-D sensor at an instant in time. Since the 1-D sensor follows perspective projection, we find that

$$\begin{bmatrix} y \\ 1 \end{bmatrix} \propto \begin{bmatrix} 0 & 1 & 0 \\ 0 & 0 & 1 \end{bmatrix} \boldsymbol{\ell} \tag{2}$$

where y is the coordinate where the direction $\boldsymbol{\ell}$ pierces the $z = 1$ plane. We observe that $[y, 1]^T \in \mathbb{P}^1$.

We must now relate the point y to its corresponding pixel location along the 1-D image. Define the v-direction to have units of pixels and to be along the 1-D image (and therefore parallel to the camera frame y-direction) as shown in Fig. 2. We then have the a similarity transformation (corresponding to part of the usual 2-D pinhole camera calibration matrix[11]) to transform from image plane coordinates to pixel coordinates

$$\begin{bmatrix} v \\ 1 \end{bmatrix} = \begin{bmatrix} d_y & v_p \\ 0 & 1 \end{bmatrix} \begin{bmatrix} y \\ 1 \end{bmatrix} \tag{3}$$

Hence, substituting Eq. (2) into Eq. (3),

$$\begin{bmatrix} v \\ 1 \end{bmatrix} \propto \begin{bmatrix} d_y & v_p \\ 0 & 1 \end{bmatrix} \begin{bmatrix} 0 & 1 & 0 \\ 0 & 0 & 1 \end{bmatrix} \boldsymbol{\ell} \tag{4}$$

$$\begin{bmatrix} v \\ 1 \end{bmatrix} \propto \begin{bmatrix} 0 & d_y & v_p \\ 0 & 0 & 1 \end{bmatrix} \boldsymbol{\ell} \tag{5}$$

We can remove the proportionality relation by introducing an explicit scaling, w,

$$\begin{bmatrix} wv \\ w \end{bmatrix} = \begin{bmatrix} 0 & d_y & v_p \\ 0 & 0 & 1 \end{bmatrix} \boldsymbol{\ell} \tag{6}$$

which happens to be $w = z$.

The unusual part of the pushbroom camera model is how to handle the second dimension (u-direction) of the 2-D pushbroom image that is formed by the motion of the camera relative to the observed scene. Suppose we collect a sequence of 1-D images with a time τ between each image. Moreover, assume that each of these 1-D images forms a column in the resulting 2-D pushbroom image. In that case, the conversion from time to pixels is given by

$$u = (t - t_0)/\tau = \Delta t/\tau \tag{7}$$

where perfect timing produces integer values of u.

A world point only appears in a particular 1-D image if it lies within the instantaneous view plane. Thus, if $\boldsymbol{v}$ is the constant velocity of the observer, then the observer's instantaneous location at the time of a particular 1-D image is

$$\boldsymbol{r} = \boldsymbol{r}_0 + \Delta t\, \boldsymbol{v} \tag{8}$$

where $\boldsymbol{r}_0$ is the observer location at time t_0. Substituting this result into Eq. (1),

$$\boldsymbol{\ell} = \boldsymbol{p} - \boldsymbol{r} = \boldsymbol{p} - (\boldsymbol{r}_0 + \Delta t\,\boldsymbol{v}) = \boldsymbol{\ell}_0 - \Delta t\,\boldsymbol{v} \qquad (9)$$

where $\boldsymbol{\ell}_0 = \boldsymbol{p} - \boldsymbol{r}_0$. Writing out the terms and constraining $\boldsymbol{\ell}$ to the instantaneous view plane (i.e., the camera y-z plane, where $\ell_x = 0$),

$$\boldsymbol{\ell} = \begin{bmatrix} 0 \\ \ell_y \\ \ell_z \end{bmatrix} = \begin{bmatrix} \ell_{0_x} \\ \ell_{0_y} \\ \ell_{0_z} \end{bmatrix} - \Delta t \begin{bmatrix} V_x \\ V_y \\ V_z \end{bmatrix} \qquad (10)$$

The first row gives us a relation between time, position, and velocity in the x-direction that allows us to determine when a point will pass through the instantaneous view plane

$$\ell_{0_x} - \Delta t\,V_x = 0 \quad \rightarrow \quad \Delta t = \ell_{0_x}/V_x \qquad (11)$$

This can be transformed to the pushbroom image u coordinate using Eq. (7)

$$u = \Delta t/\tau = \ell_{0_x}/(\tau V_x) \qquad (12)$$

or, in matrix form,

$$u = \begin{bmatrix} 1/(\tau V_x) & 0 & 0 \end{bmatrix} \boldsymbol{\ell}_0 \qquad (13)$$

To complete the camera model, we may use a similar scheme to analyze the v-coordinate of a moving pushbroom camera. Substituting Δt from Eq. (11) into Eq. (10),

$$\begin{aligned} \boldsymbol{\ell} = \begin{bmatrix} 0 \\ \ell_y \\ \ell_z \end{bmatrix} &= \begin{bmatrix} \ell_{0_x} \\ \ell_{0_y} \\ \ell_{0_z} \end{bmatrix} - \frac{\ell_{0_x}}{V_x} \begin{bmatrix} V_x \\ V_y \\ V_z \end{bmatrix} \\ &= \begin{bmatrix} 0 & 0 & 0 \\ -V_y/V_x & 1 & 0 \\ -V_z/V_x & 0 & 1 \end{bmatrix} \begin{bmatrix} \ell_{0_x} \\ \ell_{0_y} \\ \ell_{0_z} \end{bmatrix} \end{aligned} \qquad (14)$$

and further substituting into Eq. (6),

$$\begin{bmatrix} wv \\ w \end{bmatrix} = \begin{bmatrix} d_y & v_p \\ 0 & 1 \end{bmatrix} \begin{bmatrix} -V_y/V_x & 1 & 0 \\ -V_z/V_x & 0 & 1 \end{bmatrix} \boldsymbol{\ell}_0 \qquad (15)$$

Therefore, stacking Eqs. (13) and (15) yields one of the key relationships for pushbroom cameras:

$$\begin{bmatrix} u \\ wv \\ w \end{bmatrix} = \begin{bmatrix} 1/\tau & 0 & 0 \\ 0 & d_y & v_p \\ 0 & 0 & 1 \end{bmatrix} \begin{bmatrix} 1/V_x & 0 & 0 \\ -V_y/V_x & 1 & 0 \\ -V_z/V_x & 0 & 1 \end{bmatrix} \boldsymbol{\ell}_0 \qquad (16)$$

We observe here that $\boldsymbol{\ell}_0$ is the vector from the initial camera location $\boldsymbol{r}_0$ to the observed world point $\boldsymbol{p}$, all expressed in the camera frame. To write this explicitly in another frame (e.g., a Moon-fixed frame M in which elliptical crater rims are known),

$$\boldsymbol{\ell}_0 = \boldsymbol{T}_C^M (\boldsymbol{p}_M - \boldsymbol{r}_0) = \begin{bmatrix} \boldsymbol{T}_C^M & -\boldsymbol{T}_C^M \boldsymbol{r}_0 \end{bmatrix} \bar{\boldsymbol{p}}_M \qquad (17)$$

where $\boldsymbol{p}_M$ is the point expressed in the Moon-fixed frame and $\bar{\boldsymbol{p}}_M^T = [\boldsymbol{p}_M^T, 1]$. The 3×3 matrix $\boldsymbol{T}_C^M$ is the attitude transformation matrix from the Moon-fixed frame M to the pushbroom camera frame C. The relative position and orientation (sometimes called pose) of the camera relative to the Moon at time t_0 is given by the 3×4 frame transformation matrix

$$\boldsymbol{\Pi}_C^M = \begin{bmatrix} \boldsymbol{T}_C^M & -\boldsymbol{T}_C^M \boldsymbol{r}_0 \end{bmatrix} \qquad (18)$$

such that

$$\boldsymbol{\ell}_0 = \boldsymbol{\Pi}_C^M \bar{\boldsymbol{p}}_M \qquad (19)$$

Therefore, substituting into Eq. (16),

$$\begin{bmatrix} u \\ wv \\ w \end{bmatrix} = \begin{bmatrix} 1/\tau & 0 & 0 \\ 0 & d_y & v_p \\ 0 & 0 & 1 \end{bmatrix} \begin{bmatrix} 1/V_x & 0 & 0 \\ -V_y/V_x & 1 & 0 \\ -V_z/V_x & 0 & 1 \end{bmatrix} \boldsymbol{\Pi}_C^M \bar{\boldsymbol{p}}_M \qquad (20)$$

When the velocity is not purely along the camera frame x-direction and parallel to the ground, the camera motion will distort the resulting 2-D pushbroom image. In the simplest case, a vertical velocity (non-zero V_z) causes objects to appear larger or smaller and a horizontal velocity (non-zero V_y) causes image shear. This effect is illustrated in Fig. 3.

Craters as Conics on the Lunar Surface. The pushbroom camera model developed in Eq. (20) describes how a generic point $\bar{\boldsymbol{p}}_M$ in the world frame will project into an image. Suppose now that this point happens to belong to the rim of a crater. Since crater rims are well-modeled as ellipses,[8,9] we can reasonably approximate observed points belonging to a crater rim as points constrained to lie on an ellipse—or, more generally, on a conic. The elliptical (conic) crater rims are assumed to be planar features.

Without loss of generality, we define the Moon frame to have its origin at the center of the observed crater, with the Z-axis perpendicular to the plane of the crater and positive out of the surface (i.e., what someone sitting on the lunar surface would call the "up" direction). It follows that a point in the crater's plane is given by $\boldsymbol{p}_M^T = [X, Y, 0]$. Writing the 2-D location of a point on the elliptical crater rim in homogeneous coordinates as $\bar{\boldsymbol{s}}^T = [X, Y, 1] \in \mathbb{P}^2$, we see that

$$\bar{\boldsymbol{s}}^T \boldsymbol{C} \bar{\boldsymbol{s}} = 0 \qquad (21)$$

where $\boldsymbol{C}$ is a symmetric matrix of ambiguous scale (five degrees-of-freedom) describing the conic locus. An equation of this from is true regardless of the orientation of the X-axis and Y-axis within the plane of the crater. However, it is often helpful for analytical analysis, to choose our basis vectors to simplify the problem. Thus, without loss of generality, place the origin at the ellipse center and define the X-axis to be in the direction of the elliptical crater's semi-major axis. In such a situation, points along the elliptical crater rim satisfy the the constraint

$$\frac{X^2}{a^2} + \frac{Y^2}{b^2} = 1 \qquad (22)$$

where a is the semi-major axis and b is the semi-minor axis. This parameterization is general enough to describe any ellipse and leads to a conic locus matrix of the form

$$C \propto \begin{bmatrix} b^2 & 0 & 0 \\ 0 & a^2 & 0 \\ 0 & 0 & -a^2 b^2 \end{bmatrix} \quad (23)$$

The conic within the plane may be related to the 3-D geometry in a few different ways. To develop some useful relationships, begin by observing that

$$\bar{\boldsymbol{p}}_M = \begin{bmatrix} 1 & 0 & 0 \\ 0 & 1 & 0 \\ 0 & 0 & 0 \\ 0 & 0 & 1 \end{bmatrix} \bar{\boldsymbol{s}} = \boldsymbol{\Gamma} \bar{\boldsymbol{s}} \quad (24)$$
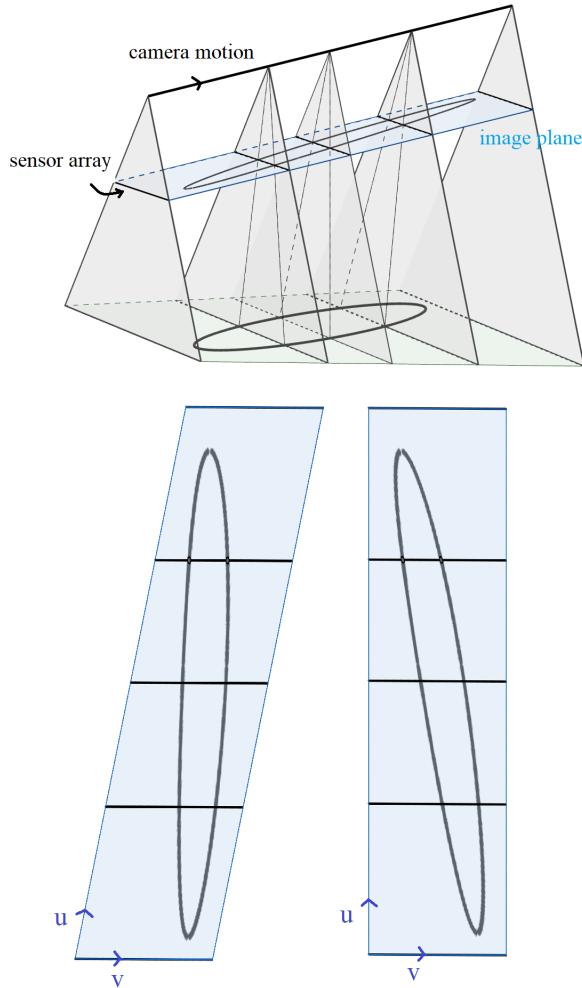
Figure 3. *The geometry of the projection on the image plane causes phenomena of shear and magnification that contributes to the appearance of the final pushbroom image.*

and, since $\boldsymbol{\Gamma}^T \boldsymbol{\Gamma} = \boldsymbol{I}_{3 \times 3}$, that

$$\bar{\boldsymbol{s}} = \boldsymbol{\Gamma}^T \bar{\boldsymbol{p}}_M \quad (25)$$

Substituting this result into Eq. (21), we find that

$$\bar{\boldsymbol{s}}^T \boldsymbol{C} \bar{\boldsymbol{s}} = \bar{\boldsymbol{p}}_M^T \boldsymbol{\Gamma} \boldsymbol{C} \boldsymbol{\Gamma}^T \bar{\boldsymbol{p}}_M = \bar{\boldsymbol{p}}_M^T \boldsymbol{Q} \bar{\boldsymbol{p}}_M \quad (26)$$

where $\boldsymbol{Q}$ is a 4×4 symmetric matrix of arbitrary scale that defines a quadric surface in $\mathbb{P}^3$.[14] Taking the intersection of this quadric with the $z = 0$ plane (i.e., the plane of the conic) leads to the conic section describing the crater rim.

The classical description of a planar conic in $\mathbb{P}^2$ familiar to most analysts was given in Eq. (21). However, there exists an alternative called the canonical parametric representation which allows us to describe the 2-D coordinates of a conic using a single parameter.[14] This representation is sometimes more convenient than Eq. (21).

We can arrive at the desired single parameter representation using a simple transformation (a homography) on the projective plane $\mathbb{P}^2$. A homography is an isomorphism describing the mapping $\mathbb{P}^n \to \mathbb{P}^n$ that is usually parameterized by an $n \times n$ matrix of arbitrary scale. Consider a point $\bar{\boldsymbol{s}} \propto [X, Y, 1] \in \mathbb{P}^2$ belonging to the elliptical crater rim and residing within the plane of the crater. Suppose there is a homography that relates $\bar{\boldsymbol{s}}$ to a corresponding point $\bar{\boldsymbol{\theta}} \propto [\psi, \theta, 1] \in \mathbb{P}^2$ in a transformed space. Thus, we may write

$$\bar{\boldsymbol{s}} \propto \boldsymbol{H} \bar{\boldsymbol{\theta}} \quad (27)$$

where $\boldsymbol{H}$ is 3×3 invertable matrix of arbitrary scale.

We know that a homography maps a conic to a conic.[8, 10] If the goal is to reduce the conic description to a single parameter, a particularly convenient choice for the transformed conic is the parabola $\psi = \theta^2$. In this case any point $\bar{\boldsymbol{\theta}}^T \propto [\psi, \theta, 1] = [\theta^2\, \theta\, 1]$ lies on the parabola and depends only on the single parameter $\theta \in \mathbb{R}$. This simple parabola can be written in terms of the usual quadric equation

$$\bar{\boldsymbol{\theta}}^T \boldsymbol{C}_\theta \bar{\boldsymbol{\theta}} = 2\theta^2 - 2\psi = 0 \quad (28)$$

where the conic locus matrix $\boldsymbol{C}_\theta$ is given by

$$\boldsymbol{C}_\theta \propto \begin{bmatrix} 0 & 0 & -1 \\ 0 & 2 & 0 \\ -1 & 0 & 0 \end{bmatrix} \quad (29)$$

The objective, therefore, is to find the homography between the transformed conic locus $\boldsymbol{C}_\theta$ and the original conic locus $\boldsymbol{C}$.

Substituting Eq. (27) into Eq. (21) yields

$$\bar{\boldsymbol{s}}^T \boldsymbol{C} \bar{\boldsymbol{s}} = \bar{\boldsymbol{\theta}}^T \boldsymbol{H}^T \boldsymbol{C} \boldsymbol{H} \bar{\boldsymbol{\theta}} = \bar{\boldsymbol{\theta}}^T \boldsymbol{C}_\theta \bar{\boldsymbol{\theta}} = 0 \quad (30)$$

so that the transformation we seek is given by

$$\boldsymbol{C}_\theta \propto \boldsymbol{H}^T \boldsymbol{C} \boldsymbol{H} \quad (31)$$

Given $\boldsymbol{C}$ from Eq. (23) and $\boldsymbol{C}_\theta$ from Eq. (31), it is straightforward to show that the homography

$$\boldsymbol{H} \propto \begin{bmatrix} a & 0 & -a \\ 0 & 2b & 0 \\ 1 & 0 & 1 \end{bmatrix} \quad (32)$$

will produce the desired anti-diagonal matrix $\boldsymbol{C}_\theta$.

Substituting the homography from Eq. (32) into Eq. (27) yields

$$\bar{\boldsymbol{s}} = \begin{bmatrix} X \\ Y \\ 1 \end{bmatrix} \propto \begin{bmatrix} a(\theta^2 - 1) \\ 2b\theta \\ \theta^2 + 1 \end{bmatrix} = \boldsymbol{H}\bar{\boldsymbol{\theta}} \qquad (33)$$

or, equivalently,

$$\bar{\boldsymbol{s}} = \frac{1}{\theta^2 + 1} \boldsymbol{H}\bar{\boldsymbol{\theta}} \qquad (34)$$

This allows us to explicitly write the (X, Y) coordinates belonging to the crater rim in terms of the parameter θ

$$X = \frac{a(\theta^2 - 1)}{\theta^2 + 1} \qquad (35a)$$

$$Y = \frac{2b\theta}{\theta^2 + 1} \qquad (35b)$$

A point around the ellipse may also be parameterized by the angle ϕ

$$X = a\cos\phi \quad \text{and} \quad Y = b\sin\phi \qquad (36)$$

which leads to

$$\cos\phi = \frac{(\theta^2 - 1)}{\theta^2 + 1} \quad \text{and} \quad \sin\phi = \frac{2\theta}{\theta^2 + 1} \qquad (37)$$

Where we observe that

$$\cot\left(\frac{\phi}{2}\right) = \frac{1 + \cos\phi}{\sin\phi} \qquad (38)$$

and substitution from Eq. (37) shows that

$$\theta = \cot(\phi/2) \qquad (39)$$

which provides a geometric understanding of how the parameter θ is related to the angle around the ellipse.

To see these representations and transformations in action, consider an ellipse with $a = 15$ and $b = 10$ as shown in Fig. 4. Choose three points A, B, C around the ellipse occurring at angles $\phi_A = 30$ deg, $\phi_B = 150$ deg, and $\phi_C = 230$ deg. Substitution into Eq. (36) gives the (X, Y) coordinates of these three points, while substitution into Eq. (39) gives the parameter θ for the same three points. The reader may verify that substitution of the values $\theta_A, \theta_B, \theta_C$ into Eq. (35a) and (35b) recovers the corresponding (X, Y) coordinates.

Conics in Pushbroom Images. Elliptical crater rims project to image conics with conventional perspective projection cameras (i.e., those that follow the pinhole camera model in both the x and y directions).[8] However, elliptical crater rims on the lunar surface do not necessarily project to conic features in a linear pushbroom image. To obtain a non-degenerate conic crater rim (e.g., ellipse) in a pushbroom image, the plane spanned by the camera y-axis and the velocity vector must be parallel to the plane of the crater. All other motion or orientations lead to either a degenerate conic or a more complicated curve (generically a polynomial of degree four as discussed in subsequent sections). That we only obtain a non-degenerate image conic under the above conditions will now be shown.

To begin, substitute Eq. (24) into Eq. (20) to find

$$\begin{bmatrix} u \\ wv \\ w \end{bmatrix} = \boldsymbol{M}\bar{\boldsymbol{s}} \qquad (40)$$

where $\boldsymbol{M}$ is the 3×3 matrix

$$\boldsymbol{M} = \begin{bmatrix} 1/\tau & 0 & 0 \\ 0 & d_y & v_p \\ 0 & 0 & 1 \end{bmatrix} \begin{bmatrix} 1/V_x & 0 & 0 \\ -V_y/V_x & 1 & 0 \\ -V_z/V_x & 0 & 1 \end{bmatrix} \boldsymbol{\Pi}_C^M \boldsymbol{\Gamma} \qquad (41)$$

Moreover, by introducing the diagonal matrix $\boldsymbol{W}$,

$$\begin{bmatrix} u \\ wv \\ w \end{bmatrix} = \begin{bmatrix} 1 & 0 & 0 \\ 0 & w & 0 \\ 0 & 0 & w \end{bmatrix} \begin{bmatrix} u \\ v \\ 1 \end{bmatrix} = \boldsymbol{W}\bar{\boldsymbol{u}} \qquad (42)$$

we see that

$$\bar{\boldsymbol{s}} = \boldsymbol{M}^{-1}\boldsymbol{W}\bar{\boldsymbol{u}} \qquad (43)$$

Observe that $\boldsymbol{M}$ is a constant matrix for any given pushbroom image, while $\boldsymbol{W}$ may be different for every point (since w may be different for every point). Proceeding undeterred, we find that

$$\bar{\boldsymbol{s}}^T \boldsymbol{C}\bar{\boldsymbol{s}} = \bar{\boldsymbol{u}}^T \boldsymbol{W}^T \boldsymbol{M}^{-T} \boldsymbol{C} \boldsymbol{M}^{-1} \boldsymbol{W}\bar{\boldsymbol{u}} = 0 \qquad (44)$$

Writing this more compactly,

$$\bar{\boldsymbol{u}}^T \boldsymbol{A}\bar{\boldsymbol{u}} = 0 \qquad (45)$$

where

$$\boldsymbol{A} = \boldsymbol{W}^T \boldsymbol{M}^{-T} \boldsymbol{C} \boldsymbol{M}^{-1} \boldsymbol{W} \qquad (46)$$

When the matrix $\boldsymbol{A}$ is constant, the points $\bar{\boldsymbol{u}}$ trace out a conic. Since $\boldsymbol{M}$ and $\boldsymbol{C}$ are constants, one obtains a conic when $\boldsymbol{W}$ is constant—and this occurs when w is constant. Consequently, we see that an elliptical crater will project to a conic in a pushbroom image when w is constant. Recall from Eq. (16), that the scaling w is given by

$$w = \ell_z = -\ell_{0_x}\frac{V_z}{V_x} + \ell_{0_z} \qquad (47)$$

The question at hand is: under what conditions is w constant? The answer has two parts. The first part considers points on the conic observed at any one instant in time. The second part considers points observed at different times. Begin by considering two points observed at the same time. When viewing a crater, the instantaneous view plane can intersect the conic in no more than two places. For the projection to be a conic in the pushbroom image, the value of w for both of these points must be the same. If two conic points are from the same instant
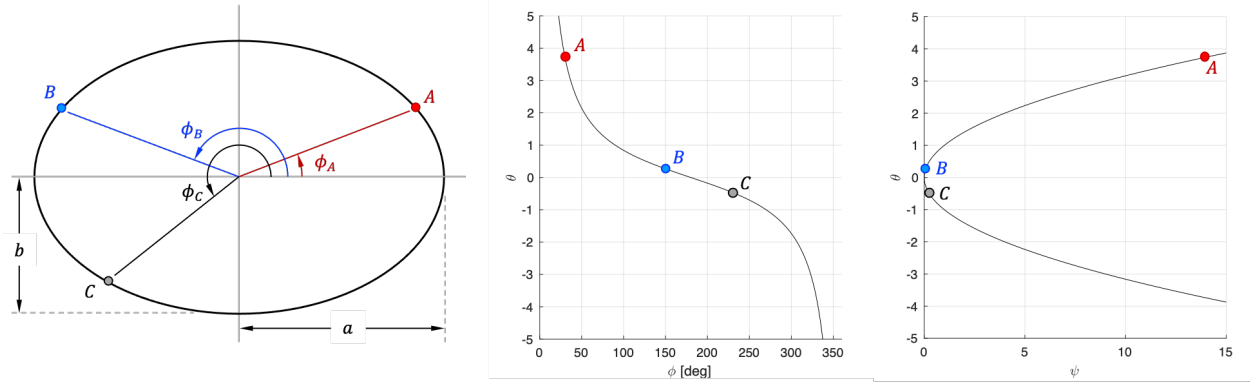
Figure 4. *The central angle which parameterizes the standard trigonometric form of an ellipse may be converted to the canonical representation parameter using a simple one-to-one cotangent mapping, and vice versa.*

in time they have the same u coordinate. Thus, from the first row of Eq. (16),

$$u = \ell_{0_{x_1}}/(\tau V_x) = \ell_{0_{x_2}}/(\tau V_x) \;\rightarrow\; \ell_{0_{x_1}} = \ell_{0_{x_2}} \qquad (48)$$

And so it follows from Eq. (47) that $\ell_{0_{z_1}} = \ell_{0_{z_2}}$. Only the ℓ_{0_y} coordinates of the two points may be different. Consequently, the line of intersection between the instantaneous view plane (i.e., camera y-z plane) and the crater plane must be purely in the camera frame y-direction. This only happens when the y-direction is parallel to the plane of the crater (i.e., when the camera x-z plane is perpendicular to the plane of the crater).

Next, consider two points observed at different times. Recall that the linear pushbroom model assumes that both the camera velocity and camera attitude are constant. It follows, therefore, that the ratio V_z/V_x is constant. Next, observe that for w to be constant from point to point means that it must be the same for two arbitrary points $\boldsymbol{p}_1$ and $\boldsymbol{p}_2$ residing on the conic. Therefore, as shown in Fig. 5, let $\boldsymbol{\ell}_{0_1}$ and $\boldsymbol{\ell}_{0_2}$ be the location of two points on the conic crater rim (and residing within the plane of the crater) relative to the camera's initial position. Substituting into Eq. (47) and assuming w is the same for both yields

$$-\ell_{0_{x_1}}\frac{V_z}{V_x} + \ell_{0_{z_1}} = w = -\ell_{0_{x_2}}\frac{V_z}{V_x} + \ell_{0_{z_2}} \qquad (49)$$

This can be rearranged to find

$$\frac{V_z}{V_x} = \frac{\ell_{0_{z_2}} - \ell_{0_{z_1}}}{\ell_{0_{x_2}} - \ell_{0_{x_1}}} = \tan\alpha \qquad (50)$$

where the angle α is shown in Fig. 5. This constraint states that the velocity vector must be parallel to the plane of the crater.

Thus, the two constraints are that both the camera frame y-direction and the velocity vector are parallel to the plane of the crater. Since $V_x \neq 0$ if the pushbroom

camera is to form a 2-D image, we know that the camera y-direction and velocity vector span a plane parallel to the crater plane. This same result may be arrived at by simplification of the implicit equation for a generic projection and is discussed in a later section.
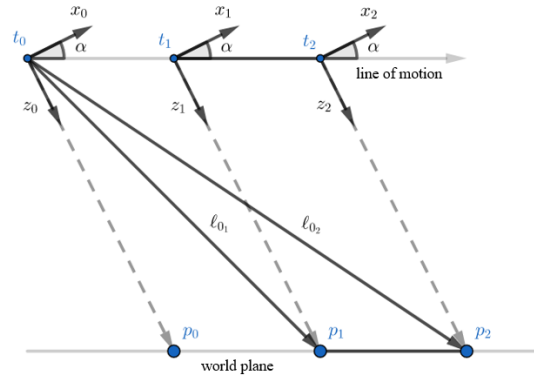
Figure 5. *Two points imaged at different time instants will have same w only if the world plane and the camera motion are parallel.*

Generic Projection of a Conic into a Pushbroom Image. We found in the prior section that an elliptical crater rim (or any other conic) will only project to another conic in a pushbroom image under very specific conditions. We now proceed to develop a more general description of the curve produced when a pushbroom camera images a conic feature.

Recalling the parametric expression of points on the conic given by Eq. (34), we now substitute this into the pushbroom projection from Eq. (40):

$$\begin{bmatrix} u \\ vw \\ w \end{bmatrix} = \frac{1}{\theta^2 + 1} \boldsymbol{M}\boldsymbol{H}\bar{\boldsymbol{\theta}} \qquad (51)$$

which expands to

$$u = \frac{A\theta^2 + B\theta + C}{\theta^2 + 1} \tag{52a}$$

$$vw = \frac{D\theta^2 + E\theta + F}{\theta^2 + 1} \tag{52b}$$

$$w = \frac{G\theta^2 + H\theta + I}{\theta^2 + 1} \tag{52c}$$

The terms $A, ..., I$ may be computed as

$$\boldsymbol{M}\boldsymbol{H} = \begin{bmatrix} A & B & C \\ D & E & F \\ G & H & I \end{bmatrix} \tag{53}$$

where $\boldsymbol{M}$ is from Eq. (41) and $\boldsymbol{H}$ is from Eq. (32). The explicit expression of these coefficients can be found in the appendix. Finally, the parametric expression of the imaged curve is

$$u = \frac{A\theta^2 + B\theta + C}{\theta^2 + 1} \tag{54a}$$

$$v = \frac{D\theta^2 + E\theta + F}{G\theta^2 + H\theta + I} \tag{54b}$$

From these equations, we can derive the implicit equation of the apparent curve in the pushbroom image. From Eq. (54a), we can write

$$(A - u)\theta^2 + B\theta + (C - u) = 0$$

and we can use it to express θ^2 as a linear function of u and θ

$$\theta^2 = \frac{(u - C) - B\theta}{(A - u)} \tag{55}$$

Substituting this expression for θ^2 in Eq. (54b) and manipulating, we obtain the expression for θ as a function of u and v

$$\theta = \frac{(u - C)(vG - D) + (vI - F)(A - u)}{B(vG - D) + (E - vH)(A - u)} \tag{56}$$

Substituting Eq. (56) into Eq. (54a) and factoring out the term $(A - u)$ the final implicit expression of the curve can can be written as a polynomial of degree 4 (a biquadric) of the form

$$\alpha u^2 v^2 + \beta u^2 v + \gamma u v^2 + \delta u v + \epsilon u^2 + \zeta v^2 + \eta u + \iota v + \kappa = 0 \tag{57}$$

where the coefficients $\alpha, ..., \kappa$ are only dependent on $A, ..., I$. The complete expression of these coefficients is written in the appendix.

Now, consider a point $\boldsymbol{\xi}^T \propto [uv, u, v, 1] \in \mathbb{P}^1 \times \mathbb{P}^1$. In this case, the polynomial from Eq. (57) can be written in compact form as

$$\bar{\boldsymbol{\xi}}^T \boldsymbol{Q} \bar{\boldsymbol{\xi}} = 0 \tag{58}$$

where $\boldsymbol{Q}$ is the 4×4 matrix of arbitrary scale

$$\boldsymbol{Q} \propto \begin{bmatrix} \alpha & \beta/2 & \gamma/2 & 0 \\ \beta/2 & \epsilon & \delta/2 & \eta/2 \\ \gamma/2 & \delta/2 & \zeta & \iota/2 \\ 0 & \eta/2 & \iota/2 & \kappa \end{bmatrix} \tag{59}$$

From here, there are a few different interesting analyses that may be performed. First is to show (again) the conditions under which a world conic projects to a conic in a pushbroom image. Second is to discuss finding the projection as an intersection of two surfaces.

Reduction to Pushbroom Conic. Consider the situation where we set the coefficients α, β and γ in Eq. (57) to zero. In this case, $\boldsymbol{Q}$ collapses to

$$\boldsymbol{Q}_0 \propto \begin{bmatrix} 0 & 0 & 0 & 0 \\ 0 & \epsilon & \delta/2 & \eta/2 \\ 0 & \delta/2 & \zeta & \iota/2 \\ 0 & \eta/2 & \iota/2 & \kappa \end{bmatrix} \propto \begin{bmatrix} 0 & \mathbf{0}_{1\times3} \\ \mathbf{0}_{3\times1} & \mathbf{A} \end{bmatrix} \tag{60}$$

where $\boldsymbol{A}$ is a 3×3 matrix of arbitrary scale

$$\boldsymbol{A} \propto \begin{bmatrix} \epsilon & \delta/2 & \eta/2 \\ \delta/2 & \zeta & \iota/2 \\ \eta/2 & \iota/2 & \kappa \end{bmatrix} \tag{61}$$

Recalling that $\bar{\boldsymbol{u}}^T = [u, v, 1] \in \mathbb{P}^2$, it follows that

$$\bar{\boldsymbol{\xi}}^T \boldsymbol{Q}_0 \bar{\boldsymbol{\xi}} = \bar{\boldsymbol{u}}^T \boldsymbol{A} \bar{\boldsymbol{u}} = 0 \tag{62}$$

where $\boldsymbol{A}$ is a constant matrix since it is made up of the constant coefficients from Eq. (57). Hence Eq. (62) describes a conic in u-v coordinates (i.e., in the pushbroom image).

Recalling from Table 2 that $\alpha = H^2 + (G - I)^2$, we find the condition for $\alpha = 0$ is only satisfied when

$$H = 0 \quad \text{and} \quad G = I \tag{63}$$

The reader may verify from Table 2 (see appendix) that this same condition also forces $\beta = 0$ and $\gamma = 0$. Imposing the two conditions of Eq. (63) is therefore necessary and sufficient to guarantee that the curve in the pushbroom image is a conic.

To better understand the meaning of Eq. (63), consider the element-wise description of the rotation matrix $\boldsymbol{T}_C^M$ given by

$$\boldsymbol{T}_C^M = \begin{bmatrix} \boldsymbol{t}_x & \boldsymbol{t}_y & \boldsymbol{t}_z \end{bmatrix} = \begin{bmatrix} T_{11} & T_{12} & T_{13} \\ T_{21} & T_{22} & T_{23} \\ T_{31} & T_{32} & T_{33} \end{bmatrix} \tag{64}$$

Using this notation, substitute the values for H, G and I from Table 1 in the appendix into Eq. (63), then the two conditions can be rewritten as

$$H = 0 \quad \rightarrow \quad \frac{T_{32}}{T_{12}} = \frac{V_z}{V_x} \tag{65a}$$

$$G = I \quad \rightarrow \quad \frac{T_{31}}{T_{11}} = \frac{V_z}{V_x} \tag{65b}$$

We can show that this pair of constraints for a world conic to project to a pushbroom conic is the same as found in earlier sections—namely that the velocity vector and camera frame y-axis span a plane parallel to the plane of the crater. This requires a few short steps. First, the

normal to the plane spanned by the velocity vector and camera frame y-axis is in the direction given by

$$\boldsymbol{v} \times \hat{\boldsymbol{y}} = \begin{bmatrix} V_x \\ V_y \\ V_z \end{bmatrix} \times \begin{bmatrix} 0 \\ 1 \\ 0 \end{bmatrix} = \begin{bmatrix} -V_z \\ 0 \\ V_x \end{bmatrix} \qquad (66)$$

and normal to the crater plane (the Moon X-Y plane) is in the direction given by

$$\boldsymbol{t}_x \times \boldsymbol{t}_y = \begin{bmatrix} T_{21}T_{32} - T_{22}T_{31} \\ T_{12}T_{31} - T_{11}T_{32} \\ T_{11}T_{22} - T_{12}T_{21} \end{bmatrix} \qquad (67)$$

If the planes are parallel then their normals are also parallel,

$$\begin{bmatrix} -V_z \\ 0 \\ V_x \end{bmatrix} = \boldsymbol{v} \times \hat{\boldsymbol{y}} \propto \boldsymbol{t}_x \times \boldsymbol{t}_y = \begin{bmatrix} T_{21}T_{32} - T_{22}T_{31} \\ T_{12}T_{31} - T_{11}T_{32} \\ T_{11}T_{22} - T_{12}T_{21} \end{bmatrix} \qquad (68)$$

Since the second row is zero (i.e., the normal vector must lie in the camera frame x-z plane) then

$$T_{12}T_{31} - T_{11}T_{32} = 0 \qquad (69)$$

which certainly agrees with Eq. (65):

$$\frac{T_{32}}{T_{12}} = \frac{V_z}{V_x} = \frac{T_{31}}{T_{11}} \rightarrow T_{12}T_{31} = T_{11}T_{32} \qquad (70)$$

However, more can be done to separately arrive at the two equations in Eq. (65). If $\boldsymbol{v}, \hat{\boldsymbol{y}}, \boldsymbol{t}_x, \boldsymbol{t}_y$ are all coplanar then their cross products are all parallel. For example,

$$\boldsymbol{v} \times \hat{\boldsymbol{y}} \propto \boldsymbol{t}_x \times \boldsymbol{t}_y \propto \boldsymbol{t}_x \times \boldsymbol{v} \propto \boldsymbol{t}_y \times \boldsymbol{v} \qquad (71)$$

It follows, therefore, that

$$\boldsymbol{t}_x \times \boldsymbol{v} = \begin{bmatrix} T_{21}V_z - T_{31}V_y \\ T_{31}V_x - T_{11}V_z \\ T_{11}V_y - T_{21}V_x \end{bmatrix} \propto \begin{bmatrix} -V_z \\ 0 \\ V_x \end{bmatrix} \qquad (72)$$

And so, from the second row, we directly reproduce Eq. (65b)

$$T_{11}V_z - T_{31}V_x = 0 \rightarrow \frac{T_{31}}{T_{11}} = \frac{V_z}{V_x} \qquad (73)$$
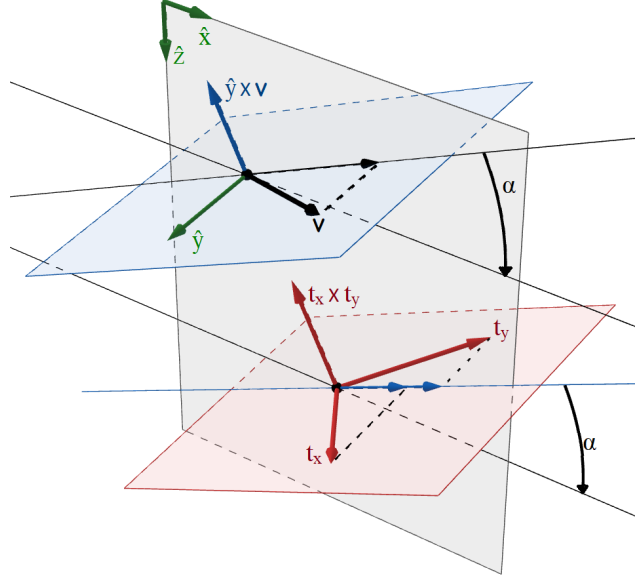
Likewise, we see that

$$\boldsymbol{t}_y \times \boldsymbol{v} = \begin{bmatrix} T_{22}V_z - T_{32}V_y \\ T_{32}V_x - T_{12}V_z \\ T_{12}V_y - T_{22}V_x \end{bmatrix} \propto \begin{bmatrix} -V_z \\ 0 \\ V_x \end{bmatrix} \qquad (74)$$

where the second row now directly reproduces Eq. (65a)

$$T_{32}V_x - T_{12}V_z = 0 \rightarrow \frac{V_z}{V_x} = \frac{T_{32}}{T_{12}} \qquad (75)$$

Thus, we see that Eq. (65) describes the situation where the velocity vector $\boldsymbol{v}$ and camera frame y-direction span a plane parallel to the crater plane (which is spanned by $\boldsymbol{t}_x$ and $\boldsymbol{t}_y$).

Figure 6. When the plane of the ellipse and the plane spanned by the velocity vector and the y-axis of the camera frame have the same normal vector, the projection of the conic in the world frame is a conic in the pushbroom image.

Generic Conic Projection as the Intersection of Curves. We now return to studying the general conic projection described by the curve of Eq. (58). First, note that since the matrix $\mathbf{Q}$ is 4×4 and symmetric, we can always associate it to a quadric in $\mathbb{P}^3$ described by the equation

$$\bar{\boldsymbol{\zeta}}^T \mathbf{Q} \bar{\boldsymbol{\zeta}} = 0 \qquad (76)$$

where $\bar{\boldsymbol{\zeta}} = [z, u, v, 1] \in \mathbb{P}^3$. The curve traced by the pushbroom camera can be formed by the intersection of this quadric with the surface $z = uv$ (i.e., the constraint on the first component of $\bar{\boldsymbol{\zeta}}$ to get $\bar{\boldsymbol{\zeta}} = \bar{\boldsymbol{\xi}}$). Orthographic projection of this 3-D curve down to the u-v plane provides the 2-D curve we seek.

To show this relationship, consider 3-D scenario illustrated in Fig. 3. In Fig. 7 we show the intersection between the quadric surface $\boldsymbol{Q}$ and the surface $z = uv$ obtained from the simulation. The intersection curve has then been projected onto the u-v plane. The matching between the projected curve and the explicit representation of Eqs. (35a) and (35b) has been shown using θ given by Eq. (39) for values of $\phi \in (0\,2\pi)$ sampled at intervals of 30 deg. This provides a way to interpret the implicit equation of the fourth degree polynomial curve given by the projection of a conic provided by a linear pushbroom camera and shows that it is equivalent to the explicit parameterization of the curve given above.

Conclusion. In this work we develop a framework to analyze how elliptical craters project into a pushbroom camera image. We consider multiple expressions for ellipses, each of which are useful in different contexts. In
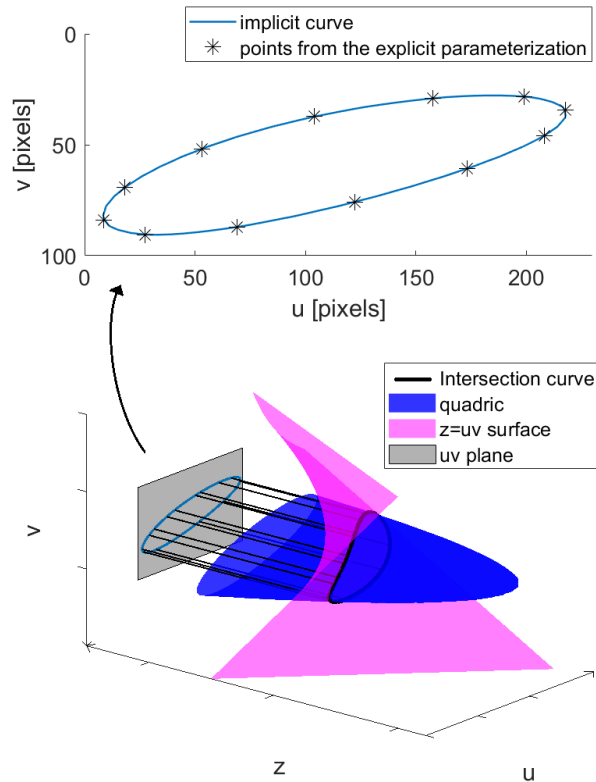
Figure 7. Interpretation of the implicit equation of the projected curve. The projection of the intersection between the quadric and the surface z=uv perfectly matches points sampled from the explicit parameterization of the curve.

addition, we relate these forms to each other via straightforward conversions. Two representations are particularly noteworthy. The first is a single-parameter explicit formulation (canonical parametric representation) conveniently maps to pushroom space via matrix multiplication of three basis vectors which are defined using common ellipse parameters (semi-major axis and semi-minor axis). Further, the pixel coordinates of the ellipse projection are easily obtained by varying the single canonical representation parameter which is shown via a practical numerical example.

The second noteworthy representation is the implicit form for the curve. In general a ellipse in the world (e.g., a crater rim) projects to a polynomial of degree four in a pushroom image. A thorough examination of the implicit form indicates that the pushroom projection happens to be another non-degenerate conic (a polynomial of degree two) when both the 1-D pushroom array (i.e., camera frame y-axis) and the camera velocity are parallel to the surface. Finally, we tie the explicit and implicit forms in the pushroom camera frame together with a numerical example. We do so by projecting the intersection between the quadric surface associated with the matrix

encoding the coefficients of the fourth order polynomial and a saddle surface onto the plane of the pushroom image to obtain the same result as the explicit form.

In summary, this paper provides an analytical framework for studying the projection of elliptical surface features (e.g., crater rims) into a pushroom camera image.

References.

[1] G. Neukum and R. Jaumann, "Hrsc: The high resolution stereo camera of mars express," in *Mars Express: The Scientific Payload*, vol. 1240, pp. 17–35, 2004.

[2] A. S. McEwen, E. M. Eliason, J. W. Bergstrom, N. T. Bridges, C. J. Hansen, W. A. Delamere, J. A. Grant, V. C. Gulick, K. E. Herkenhoff, L. Keszthelyi, R. L. Kirk, M. T. Mellon, S. W. Squyres, N. Thomas, and C. M. Weitz, "Mars reconnaissance orbiter's high resolution imaging science experiment (hirise)," *Journal of Geophysical Research: Planets*, vol. 112, no. E5, 2007. doi: 10.1029/2005JE002605.

[3] M. S. Robinson, S. M. Brylow, M. Tschimmel, D. Humm, S. J. Lawrence, P. C. Thomas, B. W. Denevi, E. Bowman-Cisneros, J. Zerr, M. A. Ravine, M. A. Caplinger, F. T. Ghaemi, J. A. Schaffner, M. C. Malin, P. Mahanti, A. Bartels, J. Anderson, T. N. Tran, E. M. Eliason, A. S. McEwen, E. Turtle, B. L. Jolliff, and H. Hiesinger, "Lunar reconnaissance orbiter camera (lroc) instrument overview," *Space Science Reviews*, vol. 150, pp. 81–124, 1 2010. doi: 10.1007/s11214-010-9634-2.

[4] J. R. Jensen, *Remote Sensing of the Environment: An Earth Resource Perspective*. Prentice Hall Series in Geographic Information Science, Pearson Prentice Hall, 2nd ed., 2007.

[5] M. Robinson, "Lro moon lroc 2 edr v1.0," 2010. doi: 10.17189/1520250.

[6] S. Robbins, "A new global database of lunar impact craters > 1–2 km: 1. crater locations and sizes, comparisons with published databases, and global analysis," *Journal of Geophysical Research: Planets*, vol. 124, pp. 871–892, 2018. doi: 10.1029/2018JE005592.

[7] A. Lagain and et al., "Mars crater database: A participative project for the classification of the morphological characteristics of large martian craters," in *Large Meteorite Impacts and Planetary Evolution VI*, pp. 629–644, Geological Society of America, 2021. doi: 10.1130/2021.2550(29).

[8] J. A. Christian, H. Derksen, and R. Watkins, "Lunar crater identification in digital images," *The Journal of the Astronautical Sciences*, vol. 68, no. 4, pp. 1056–1144, 2021. doi: 10.1007/s40295-021-00287-8.

[9] W. Bottke, S. Love, D. Tytell, and T. Glotch, "Interpreting the elliptical crater populations on mars, venus, and the moon," *Icarus*, vol. 145, pp. 108–121, 2000. doi: 10.1006/icar.1999.6323.

[10] R. Hartley and A. Zisserman, *Multiple View Geometry in Computer Vision*. USA: Cambridge University Press, 2 ed., 2003. doi: 10.1017/CBO9780511811685.

[11] J. A. Christian, "A Tutorial on Horizon-Based Optical Navigation and Attitude Determination with Space Imaging Systems," *IEEE Access*, pp. 19,819–19,853, 2021. doi: 10.1109/ACCESS.2021.3051914.

[12] R. Gupta and R. Hartley, "Camera estimation for orbiting pushbrooms," *Proc. Second Asian Conf. Computer Vision*, (Singapore), Dec. 1995.

[13] R. Gupta and R. I. Hartley, "Linear pushbroom cameras," *IEEE Transactions on Pattern Analysis and Machine Intelligence*, vol. 19, no. 9, pp. 963–975, 1997. doi: 10.1109/34.615446.

[14] J. G. Semple and G. T. Kneebone, *Algebraic Projective Geometry*. Oxford: Oxford University Press, 1952.

Appendix.

Table 1. Coefficients for the explicit form. We are using the element-wise description of T_C^M as given in Eq. (64). **Note:** $r_{0,c} = T_C^M r_0$

A	$\frac{1}{\tau V_x}(aT_{11} - r_{0x,C})$
B	$\frac{1}{\tau V_x}(2bT_{12})$
C	$\frac{1}{\tau V_x}(-aT_{11} - r_{0x,C})$
D	$d_y\left(-\frac{V_y}{V_x}(aT_{11} - r_{0x,c}) + aT_{21} - r_{0y,c}\right) + v_p\left(-\frac{V_z}{V_x}(aT_{11} - r_{0x,C}) + aT_{31} - r_{0z,C}\right)$
E	$d_y\left(-\frac{V_y}{V_x}2bT_{12} + 2bT_{22}\right) + v_p\left(-\frac{V_z}{V_x}2bT_{12} + 2bT_{32}\right)$
F	$d_y\left(-\frac{V_y}{V_x}(-aT_{11} - r_{0x,C}) - aT_{21} - r_{0y,C}\right) + v_p\left(-\frac{V_z}{V_x}(-aT_{11} - r_{0x,C}) - aT_{31} - r_{0z,C}\right)$
G	$-\frac{V_z}{V_x}(aT_{11} - r_{0x,C}) + aT_{31} - r_{0z,C}$
H	$-\frac{V_z}{V_x}2bT_{12} + 2bT_{32}$
I	$\frac{V_z}{V_x}(aT_{11} + r_{0x,C}) - aT_{31} - r_{0z,C}$

Table 2. Coefficients for the implicit form.

α	$H^2 + (G-I)^2$
β	$-2EH - 2(D-F)(G-I)$
γ	$2(AI - CG)(G-I) - CH^2 - AH^2 + BGH + BHI$
δ	$2AEH - 2(AI - CG)(D-F) - 2(AF - CD)(G-I) - BDH - BEG - BEI - BFH + 2CEH$
ϵ	$E^2 + (D-F)^2$
ζ	$2(AF - CD)(D-F) - CE^2 - AE^2 + BDE + BEF$
η	$C(AH^2 - 2BGH) + (AI - CG)^2 + B^2GI - ABHI + BCGH$
ι	$C(2BDH - 2AEH + 2BEG) - 2(AF - CD)(AI - CG) - B^2DI - B^2FG + ABEI + ABFH - BCDH - BCEG$
κ	$C(AE^2 - 2BDE) + (AF - CD)^2 + B^2DF - ABEF + BCDE$